


## Immune priming and induction of tertiary lymphoid structures in a cord-blood humanized mouse model of gastrointestinal stromal tumor

Bo He<sup>a\*</sup>, Larissa Dymond<sup>b\*</sup>, Kira H. Wood<sup>a</sup>, Edward R. Bastow<sup>a</sup>, Jiulia Satiaputra<sup>a</sup>, Ji Li<sup>a</sup>, Anna Johansson-Percival<sup>a</sup>, Juliana Hamzah<sup>c</sup>, M. Priyanthi Kumarasinghe<sup>d</sup>, Mohammed Ballal<sup>e,f</sup>, Jonathan Foo<sup>f,g</sup>, Mikael Johansson<sup>g</sup>, Hooi C. Ee<sup>g,h</sup>, Scott W. White<sup>i</sup>, Louise Winteringham<sup>b</sup>, and Ruth Ganss<sup>i</sup> 

<sup>a</sup>Cancer Microenvironment Laboratory, Harry Perkins Institute of Medical Research, QEII Medical Centre and Centre for Medical Research, The University of Western Australia, Perth, Western Australia, Australia; <sup>b</sup>Translational Cancer Research Program, Harry Perkins Institute of Medical Research, QEII Medical Centre and Centre for Medical Research, The University of Western Australia, Perth, Western Australia, Australia; <sup>c</sup>Imaging & Therapy Laboratory, Harry Perkins Institute of Medical Research, QEII Medical Centre and Centre for Medical Research, The University of Western Australia, Perth, Western Australia, Australia; <sup>d</sup>Department of Anatomical Pathology, PathWest QEII Medical Centre, Perth, Western Australia; <sup>e</sup>Department of General Surgery, Fiona Stanley Hospital, Western Australia, Australia; <sup>f</sup>Division of Surgery, School of Medicine, University of Western Australia, Western Australia, Australia; <sup>g</sup>Sir Charles Gairdner Hospital, QEII Medical Centre, Perth, Western Australia, Australia; <sup>h</sup>Division of Internal Medicine, School of Medicine, University of Western Australia, Western Australia, Australia; <sup>i</sup>Division of Obstetrics and Gynaecology, Faculty of Medicine, Dentistry, and Health Sciences, The University of Western Australia, Perth, Western Australia, Australia

### ABSTRACT

Gastrointestinal stromal tumors (GISTs) harbor diverse immune cell populations but so far immunotherapy in patients has been disappointing. Here, we established cord blood humanized mouse models of localized and disseminated GIST to explore the remodeling of the tumor environment for improved immunotherapy. Specifically, we assessed the ability of a cancer vascular targeting peptide (VTP) to bind to mouse and patient GIST angiogenic blood vessels and deliver the TNF superfamily member LIGHT (TNFS14) into tumors. LIGHT-VTP treatment of GIST in humanized mice improved vascular function and tumor oxygenation, which correlated with an overall increase in intratumoral human effector T cells. Concomitant with LIGHT-mediated vascular remodeling, we observed intratumoral high endothelial venules (HEVs) and tertiary lymphoid structures (TLS), which resemble spontaneous TLS found in GIST patients. Thus, by overcoming the limitations of immunodeficient xenograft models, we demonstrate the therapeutic feasibility of vascular targeting and immune priming in human GIST. Since TLS positively correlate with patient prognosis and improved response to immune checkpoint inhibition, vascular LIGHT targeting in GIST is a highly translatable approach to improve immunotherapeutic outcomes.

### ARTICLE HISTORY

Received 23 July 2024  
Revised 16 September 2024  
Accepted 16 September 2024

### KEYWORDS



Gastrointestinal tumor (GIST); humanized mice; LIGHT (TNFS14); tertiary lymphoid structures (TLS); vascular targeting

## Introduction


Gastrointestinal stromal tumors (GISTs) are sarcomas that arise along the gastrointestinal tract. In most GIST, mutant forms of the proto-oncogene *c-KIT* (tyrosine protein kinase *KIT*; *CD117*) or platelet-derived growth factor receptor alpha (*PDGFRA*) drive proliferation and tumor progression. Current treatments comprise surgical resection and tyrosine kinase inhibitor (TKI) treatment such as imatinib mesylate (Gleevec) with high affinity to *c-KIT* and *PDGFRA*.<sup>1</sup> While most patients respond well to TKI treatment, drug resistance ultimately leads to tumor progression, demonstrating the need for alternative treatment options.<sup>2</sup> More recently, immunotherapies such as immune checkpoint inhibitors alone or in combination with TKIs have been explored in clinical trials with mixed results.<sup>3,4</sup> The use of checkpoint inhibition in GIST is supported by histopathological findings which show an abundance of T lymphocytes, particularly in metastatic lesions,<sup>5</sup> some high densities of *CD3*<sup>+</sup> tumor-infiltrating lymphocytes as predictors of progression-free

survival,<sup>6</sup> and in *in silico* analyses.<sup>7</sup> Moreover, in a *c-KIT* mutant transgenic mouse model, T cells critically enhance the anti-tumor effects of imatinib.<sup>8</sup> In the same model, receptor programmed death 1 (PD-1)/programmed death 1 ligand (PD-L1) inhibition when combined with imatinib further increases T cell effector function.<sup>9</sup> Interestingly, primary GISTs can also harbor immune cell clusters that are organized into tertiary lymphoid structures (TLS)<sup>10</sup>; these spontaneous, intratumoral TLS support T cell entry and priming, and confer a positive prognosis in most cancers.<sup>11</sup> In GIST patients, the presence of TLS correlates with smaller tumor size and is an independent prognostic parameter.<sup>10</sup>

Overall, these findings encourage the development of immunotherapeutic approaches in GIST, which harness the adaptive immune system and potentially increase the formation and frequency of TLS. Therapeutic induction of TLS in cancer, however, remains challenging. We have previously shown in syngeneic pancreatic and brain cancer models that

**CONTACT** Ruth Ganss  [ganss@perkins.org.au](mailto:ganss@perkins.org.au)  Cancer Microenvironment Laboratory, Harry Perkins Institute of Medical Research, 6 Verdun Street, Nedlands, Perth, Western Australia 6009, Australia

\*Equal contributions.

 Supplemental data for this article can be accessed online at <https://doi.org/10.1080/2162402X.2024.2406576>

© 2024 The Author(s). Published with license by Taylor & Francis Group, LLC.

This is an Open Access article distributed under the terms of the Creative Commons Attribution-NonCommercial License (<http://creativecommons.org/licenses/by-nc/4.0/>), which permits unrestricted non-commercial use, distribution, and reproduction in any medium, provided the original work is properly cited. The terms on which this article has been published allow the posting of the Accepted Manuscript in a repository by the author(s) or with their consent.

the compound LIGHT-VTP, a fusion of the tumor necrosis factor superfamily TNFS14 (LIGHT) with a vascular targeting peptide (VTP), restores tumor perfusion by “normalizing” angiogenic blood vessels, attracts T cells into the tumor micro-environment, and induces intratumoral TLS.<sup>12–14</sup> Mechanistically, vessel normalization by LIGHT-VTP occurs by inducing pericyte maturation, which in turn leads to tighter alignment of pericytes with endothelial cells and overall improvement of vascular function.<sup>15</sup> Once a critical lymphocyte density is reached intratumorally, so-called high endothelial venules (HEVs) can arise and facilitate further lymphocyte clustering into TLS.<sup>14,16</sup>

To assess the vascular and immune-modulatory potential of LIGHT-VTP specifically in GIST, we generated a mouse model where human GIST cells were implanted into cord-blood humanized mice carrying a functional human adaptive immune system.<sup>17,18</sup> We compared the immune landscape of subcutaneously (s.c.) implanted, primary GIST and an intraperitoneal (i.p.) GIST model, mimicking metastases in humanized mice, to human primary GIST specimens. We also demonstrate *ex vivo* efficacy of vascular peptide binding in angiogenic blood vessels of mouse and human GIST. *In vivo* treatment of GIST-bearing humanized mice with LIGHT-VTP resulted in a high tumor vessel normalization index and immune score concomitant with the induction of TLS. This demonstrates the feasibility of vessel-targeted immunotherapy in GIST with the potential to improve on current immunotherapeutic options.

## Material and methods

### Cell lines

The human GIST-T1 cell line was purchased from COSMO BIO USA (United Bio Research, Australia, PMC-GISTM-COS). The GIST-T1 cell line was established from a pleural metastasis of a gastrointestinal stromal tumor (GIST) of the stomach as published.<sup>19</sup> Cells were cultured in Dulbecco’s Modified Eagle Medium (DMEM) supplemented with 10% fetal calf serum (FCS), 100 units/ml penicillin/100 µg/ml streptomycin, and 2 mM L-glutamine (Thermo Fisher Scientific).

### GIST patients

Fresh human GISTs were collected with patient consent at the time of surgical resection. Gastric GIST with c-KIT mutations from three male and one female patients were used (for patient summary, see Supplementary Table 1). Tissue collection was approved by the Sir Charles Gairdner Group and Fiona Stanley Hospital Human Research Ethics Committees, Western Australia, Australia (RGS0000000919).

### Cord blood processing and isolation of human CD34<sup>+</sup> stem cells

Human umbilical cord blood was collected from informed and consenting donors at King Edward Memorial Hospital, Western Australia. Approval to collect and use donated stem cells was obtained from the Women and Newborn Health

Service Ethics Committee (RGS0000000376). Cord blood was collected into a sterile collection bag (Macopharma) containing 21 ml of citrate phosphate dextrose solution. The collection volume varied between 45 and 166 ml. Mononuclear cells were purified from the cord blood by density centrifugation with Lymphoprep (StemCell Technologies) or Ficoll® Paque Plus (Cytiva). Human CD34<sup>+</sup> cells were enriched by positive magnetic separation using the human CD34 MicroBead Ultrapure Kit, LS columns and a magnetic separator (Miltenyi Biotec) as per the manufacturer’s instructions. An additional labeling and column separation step was performed to increase the purity of the CD34<sup>+</sup> cell isolates.<sup>20</sup> The purity of CD34<sup>+</sup> cell isolates was determined by flow cytometry on a BD FACSAria II or Cytex Aurora, using anti-huCD34-FITC and anti-huCD45-APC antibodies (StemCell Technologies). Samples were incubated with DAPI or ViaDye Violet (Cytex Biosciences) to allow exclusion of dead cells, and nucleated cells were selected by light scatter. Samples with ≥ 75% CD34<sup>+</sup> cells were used for generating humanized mice.

### Generation of humanized mice

NSG mice (NOD.Cg-Prkdc<sup>scid</sup>Il2rg<sup>tm1Wjl</sup>/SzJ) were purchased from Ozgene, Western Australia. Mice were maintained under specific pathogen-free conditions, and all experiments were approved by the Harry Perkins Institute of Medical Research Animal Ethics Committee (AE077, AE253, AE254). Newborn (within 2 days of birth), or 4–6 week old juvenile NSG mice received 100 cGy (newborn-5 weeks) or 250 cGy (6 weeks) total body irradiation using a Linear Accelerator (Varian Truebeam). Mice were injected with CD34<sup>+</sup> cells 18–24 hours after irradiation. Newborns received 50,000 CD34<sup>+</sup> cells via the facial vein, while older mice received 100,000 CD34<sup>+</sup> cells via the tail vein. Human hematopoietic chimerism was evaluated with flow cytometry of peripheral blood using human and mouse CD45 antibodies (msCD45-PerCP-Cy5.5, huCD45-APC-Cy7, BD Biosciences). Human B cells (huCD19-AF647, BioLegend), T cells (huCD3-BB515, huCD4-PE-CF594, huCD8-PE-Cy7), monocytes (huCD14-PE), and NK cells (huCD56-BV421), all from BD Biosciences, were also evaluated at 16 weeks. Red blood cells were lysed using BD Pharm Lyse (BD Biosciences), and samples were blocked for nonspecific staining using Mouse BD Fc Block (BD Biosciences), True-Stain Monocyte Blocker (BioLegend), and Brilliant Stain Buffer (BD Biosciences), as per manufacturers’ instructions. Human hematopoietic chimerism percentage was calculated as huCD45/(msCD45 + huCD45), and mice were considered successfully humanized if huCD45<sup>+</sup> cell numbers were 25% or above at 16 weeks post-injection. Mice were subsequently distributed into equivalent experimental and control groups based on chimerism.<sup>21</sup>

### LIGHT-VTP production

Recombinant murine LIGHT (aa 58–220, 17 kDa) with C-terminal CGKRK was produced in *E. coli* as previously described.<sup>15</sup> Mature human LIGHT (aa 74–240, 18 kDa, with C-terminal CGKRK peptide, connected via a GGG linker) was cloned into Xho/BamH1 sites of the vector pET-44a (Novagen)

to express a soluble fusion protein with N-terminal Nus•Tag/His•Tag and purified as described.<sup>15</sup>

### Tumor injection and treatment

Tumors were implanted into humanized mice 17–24 weeks post-injection of CD34<sup>+</sup> cells. For s.c. tumors, GIST-T1 cells were mixed 1:1 with growth medium and Matrigel (BD Biosciences) on ice, and  $1 \times 10^6$  cells were injected into the right flank. LIGHT-VTP which consisted of a 1:1 mixture of 20 ng of human and mouse LIGHT-VTP was diluted in PBS and i.v. injected 2×/week via the tail vein when tumors reached 110–160 mm<sup>3</sup>. Controls received PBS only. Mice were euthanized when tumors reached 400–600 mm<sup>3</sup>. For i.p. tumors,  $1 \times 10^6$  GIST cells in 100–200  $\mu$ L PBS were injected via intraperitoneal injection. Treatments commenced after 6–8 weeks of growth with injections of 20 ng of human and mouse LIGHT-VTP 2×/week via the tail vein. Mice were euthanized after 8–11 weeks of growth. Prior to sacrifice, some mice were i.v. injected with 50  $\mu$ g FITC-labeled tomato lectin (*Lycopersicon esculentum*, Vector, circulated for 5 min) and/or pimonidazole (i.p., 60 mg/kg, circulated for 60 min, Hypoxyprobe<sup>TM</sup>-1 Kit, Hypoxyprobe, Inc., USA). Mice were perfused with 2% formalin, before tumors were excised and placed in cold sucrose on ice (10% sucrose for 2 h, 30% sucrose overnight). Some tumors were collected in FACS buffer for flow cytometry analysis.

### Histology and immunohistochemistry (IHC)

GIST tumors were frozen in OCT compound (Tissue Tek). Ice-cold acetone was used to fix 7- $\mu$ m frozen sections. Hematoxylin and eosin (H&E) staining was performed on frozen sections using hematoxylin Gill3 and eosinY (Merck). Sections were stained with primary antibodies (anti-huCD31, Dako; anti-msCD31, BD Biosciences; anti-PNAd, MECA79, BD Biosciences; anti-huCD3, Abcam; anti-huCD20, anti-CD68, both Thermo Fisher Scientific; anti-CD68-AF594, BioLegend; anti-CD56, BioRad; anti-SMA, alpha, Sigma). Primary antibodies were detected using secondary antibodies (anti-rabbit IgG-AF488, anti-rat IgG-AF594, both Thermo Fisher Scientific; anti-mouse DyLight 405, Jackson ImmunoResearch Labs) or mouse-on-mouse (MOM) kit (Vector). DAPI was used in some tissues to visualize cell nuclei. Hypoxia was quantified in mice treated with pimonidazole using anti-pimonidazole antibody (Hypoxyprobe Inc., USA). A Nikon Ti-E microscope and NIS software (Nikon, version 4.0) were used for image analysis. At least three mice or tumors were analyzed per treatment group; 5–15 images per tumor were analyzed. All material summarized in one graph was imaged with standardized threshold intensity. Positively stained features are expressed as % marker expression compared to total tumor surface area in one image (surface area %). Alternatively, co-localization was measured as fluorescence intensity ratio between red and green fluorescence channels or % overlay of red/green fluorescence.

### Peptide binding assay

Linear VTP peptide CGKRK (FAM-X-CGKRK) was synthesized as described<sup>21</sup> and labeled with a 5(6)-carboxyfluorescein (FAM) separated by a 6-aminohexanoic acid spacer (X). Seven  $\mu$ m frozen tumor sections were fixed in ice-cold acetone, air dried, and incubated in Tris-buffered saline (TBS)/4% FCS for 30 min, followed by avidin/biotin blocking (Vector) for 15 min. Sections were incubated with 0.1  $\mu$ M of CGKRK-FAM peptide in 0.5% FBS for 1 h at RT, followed by washing in TBS and incubation with biotinylated goat anti-FITC antibody for 40 min (Abcam); signals were amplified using streptavidin-horseradish peroxidase conjugates (SA-HRP) following the manufacturer's instructions (tyramide amplification kit, ThermoFisher). Before mounting with anti-fade mounting medium with DAPI (Vector), sections were incubated with an autofluorescence quenching kit (Vector) for 2 min.

### Intratumoral flow cytometry analysis

For flow cytometry analysis, tumors were harvested in FACS buffer (1% FCS in PBS) and digested in 2.5 ml/0.1 g tumor of 100 U/ml Collagenase IV, 0.5 mg/ml DNase I (both Worthington Biochemical) in PBS. Cell suspensions were stained with ViaDye (Cytex) for live cell detection.  $5 \times 10^6$  cells were blocked with Fc-block (CD16/CD32, clone 2.4G2, BioXCell) for 15 min on ice and subsequently stained for 30 min on ice in FACS buffer with the following anti-human antibodies: anti-CD45-PE, anti-CD3-AF488, anti-CD4-BUV737, anti-CD8-APC-H7, anti-CD25-PE, anti-GrzB-PE, anti-Ki67-PE-Cy7 (all BD Biosciences), anti-FOXP3-APC (ThermoFisher), and anti-CD19-AF647 (BioLegend). The True-Nuclear Transcription Factor Buffer Set (BioLegend) was used for all intracellular staining. After two washes in permeabilization buffer, cells were analyzed using the BD FACSAria II (BD Biosciences) and DIVA software (BD Biosciences). For all samples, 50,000–500,000 live singlets were analyzed.

### Statistical analysis

GraphPad Prism software (version 10) was used for statistical analyses. Data are presented as mean  $\pm$  SEM. Numbers (*n*) of mice and *p* values are shown in figure legends. For comparison of groups, one-way ANOVA with *post hoc* Tukey testing or two-tailed unpaired Student's *t*-tests were used as indicated in figure legends. *p* values <0.05 were considered significant.

## Results

### Cord blood humanized mice develop a human adaptive immune system

To generate humanized mice for tumor engraftment, NSG mice were irradiated and injected with freshly purified CD34<sup>+</sup> hematopoietic stem cells from human cord blood (Figure 1a). Mice were analyzed at 12, 16, and 36 weeks post-engraftment for the presence of human CD45<sup>+</sup> immune cells in peripheral blood (Figure 1b and Supplementary Figure S1). The percentage of mice with

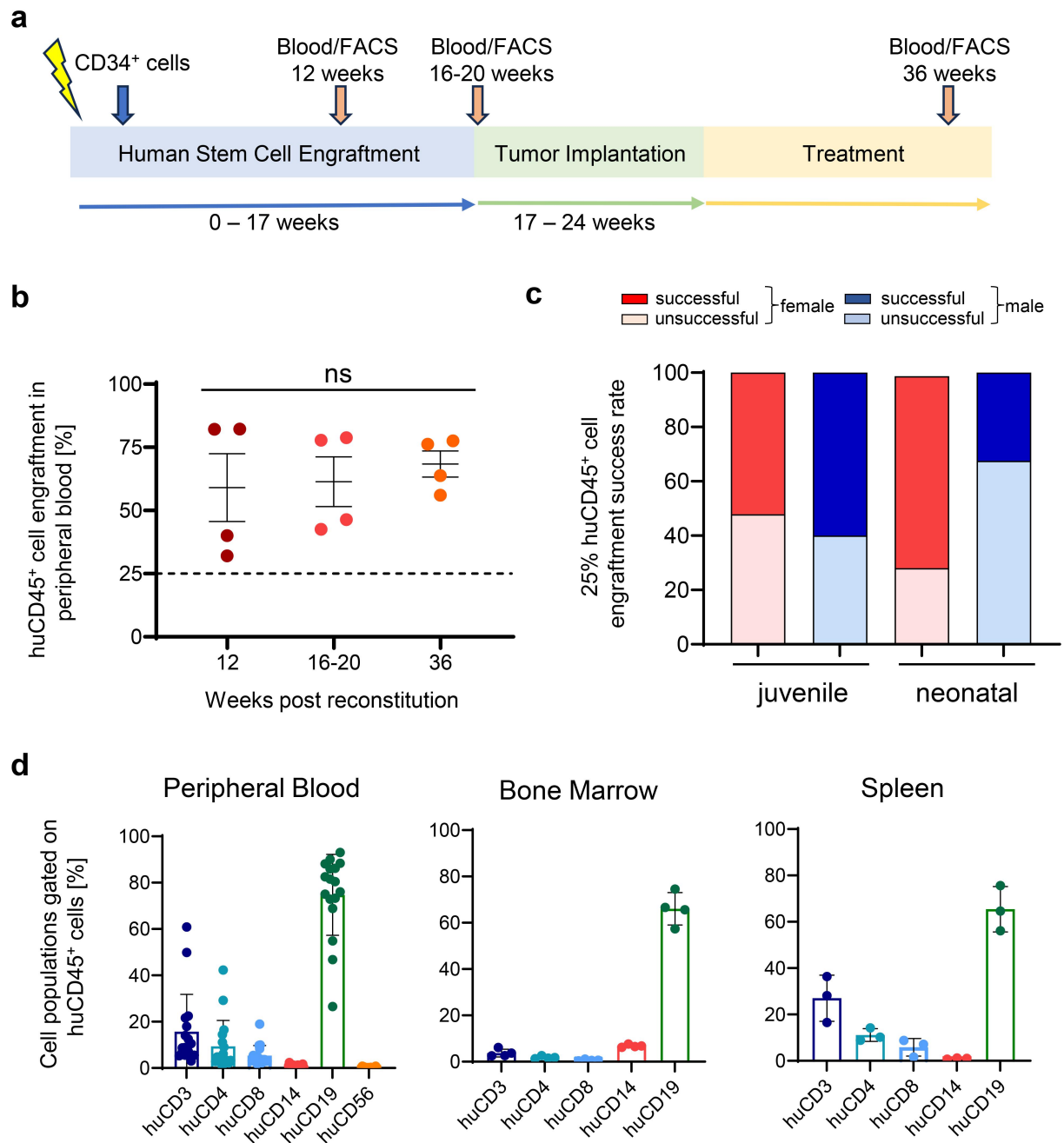


**Figure 1.** Cord blood humanized NSG mice harbor a human adaptive immune system. (a) Generation of humanized mice, analysis of peripheral blood, and tumor implantation timeline. (b) Longitudinal analysis of huCD45<sup>+</sup> cells in peripheral blood following stem cell engraftment,  $n = 4$  mice, ns, not statistically significant. (c) Engraftment success rate (>25% of huCD45<sup>+</sup> cells in peripheral blood) in juvenile females ( $n = 44$ )/males ( $n = 5$ ) and neonatal females ( $n = 75$ )/males ( $n = 77$ ) at 16 weeks post stem cell injection. (d) Percent human CD3<sup>+</sup>, CD4<sup>+</sup>, CD8<sup>+</sup>, CD14<sup>+</sup>, CD19<sup>+</sup>, and CD56<sup>+</sup> cells in peripheral blood (left),  $n = 17$  mice, bone marrow (middle),  $n = 4$  mice, and spleen (right),  $n = 3$  mice.

successful (>25%) human engraftment was dependent on the age and sex of the mice at the time of radiation and stem cell injection with the best performance achieved in neonatal female mice (Figure 1c). Furthermore, blood, spleen, and bone marrow at 16 weeks post-engraftment demonstrated the presence of major adaptive human immune cell subpopulations such as CD3<sup>+</sup>, CD4<sup>+</sup> and CD8<sup>+</sup> T cells, CD19<sup>+</sup> B cells, and to a lesser extent CD14<sup>+</sup> monocytes and CD56<sup>+</sup> NK cells within human CD45<sup>+</sup> cell populations (Figure 1d). Male and female mice from all groups reaching a human CD45<sup>+</sup> cell engraftment of >25%

at week 16 were considered “humanized” and enrolled in subsequent experiments, including s.c. and i.p. GIST implantations and LIGHT-VTP treatments.

#### **Intraperitoneal GISTs in humanized mice are infiltrated by human CD3<sup>+</sup> T cells**

Humanized NSG mice were s.c. implanted with GIST-T1 cells, a c-KIT mutant human cell line, 17–24 weeks after stem cell engraftment to generate a model of locally restricted, primary tumor growth. Alternatively, mice were injected i.p. with



GIST-T1 cells for a model of disseminated tumor growth, consistent with the peritoneum being a common GIST metastatic site.<sup>22</sup> S.c. tumor growth rate in humanized NSG mice was comparable to non-humanized NSG mice (Supplementary Figure S2a). S.c. tumors at 400–600 mm<sup>3</sup> and i.p. tumors at 8–11 weeks after tumor implantation were analyzed for morphology as well as vascular and immune features in comparison with human primary gastric GIST specimens (Figure 2). The microscopic appearance of GIST is site-dependent with most human GIST being spindle cell tumors, followed by a mixed phenotype of epithelioid and spindle cell morphology or epithelioid phenotype only.<sup>23</sup> H&E staining of s.c. and i.p.

mouse GISTs shows features of a mixed phenotype which was matched with a human GIST with similar features (Figure 2a, Supplementary Table 1). While CD31<sup>+</sup> blood vessels in mouse GIST are smaller than their human counterparts, staining with the pericyte marker alpha smooth muscle actin ( $\alpha$ SMA or ACTA2) revealed similar vessel coverage of approximately 50% of all vessels (Figure 2b). In contrast to s.c. GISTs which harbor only a few human CD3<sup>+</sup> T cells, i.p. GISTs were moderately infiltrated; T cell infiltration in human gastric GIST is highly variable and a moderately infiltrated example is depicted in Figure 2c. Human B cells (CD20) were detectable but are not abundant in mouse or human GIST specimens (Figure 2d).

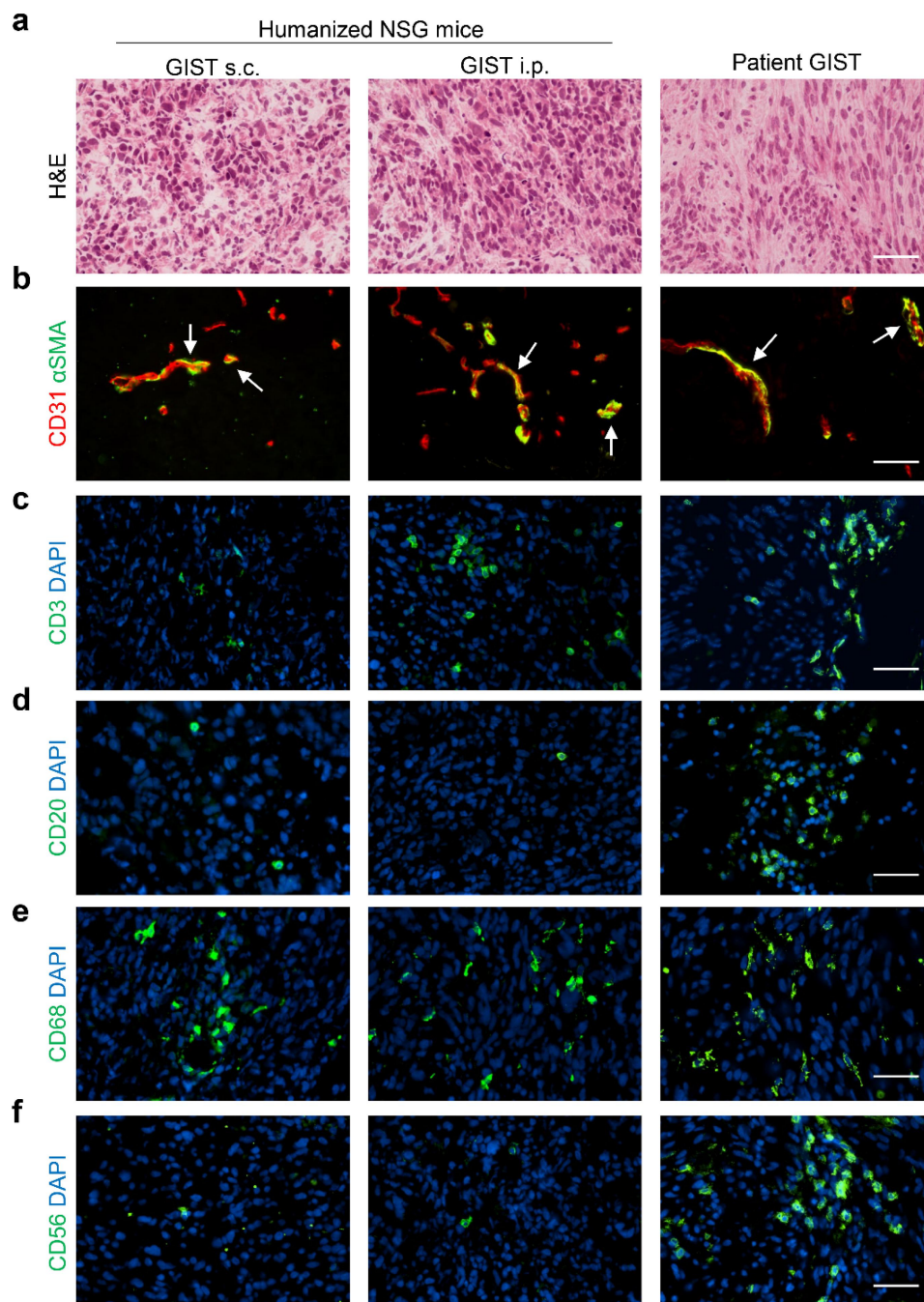


**Figure 2.** GISTs grown in humanized mice differ in some human immune cell content compared to patient GIST. (a) Representative H&E images of GISTs grown s.c. or i.p. in humanized mice, or a patient GIST. (b) Appearance of blood vessels (CD31, red) covered by pericytes ( $\alpha$ SMA, green, arrows). (c–f) Representative images of (c) CD3<sup>+</sup> T cell, (d) CD20<sup>+</sup> B cell, (e) CD68<sup>+</sup> macrophage, and (f) CD56<sup>+</sup> NK cell infiltration in GISTs. Scale bar, 50  $\mu$ m.

Human CD68<sup>+</sup> macrophages diffusely infiltrate both mouse and human GISTs (Figure 2e). However, while human GISTs were consistently positive for human NK cells (CD56), these cells were rare in GISTs grown in humanized mice (Figure 2f). Overall, the most significant difference between mouse and human GIST was the lack of infiltrating NK cells in mice, consistent with a preferential lymphoid engraftment in humanized NSG mice.<sup>24</sup> In addition, mouse GISTs of the peritoneum were infiltrated with human CD3<sup>+</sup> T cells similar to human gastric GIST which is in contrast to s.c. local GIST.

### **GIST blood vessels are targets for the CGKRK vascular binding peptide**

Angiogenic tumor blood vessels are highly abnormal, a feature which can be exploited to specifically deliver payloads into tumors.<sup>25</sup> The small peptide CGKRK is one of several VTPs that specifically target tumor vasculature with no binding activity to blood vessels in normal organs, as shown for instance in mouse and human glioblastoma.<sup>12,21</sup> To test the binding capacity of VTP (CGKRK) on mouse and human GIST specimens *ex vivo*, FAM-labeled peptide was incubated with fresh frozen tumor sections, and binding to CD31<sup>+</sup> tumor vessels was quantified. As shown in Figure 3, 80–90% of human GIST blood vessels were covered by VTP. While mouse GIST blood vessels are considerably smaller, VTP coverage of vessels ranges from 60 to 80% indicating that vascular targeting of GIST is a viable approach across species. Subsequently, a fusion protein combining the cytokine LIGHT with VTP was used to modulate the GIST environment and attract immune cells.

### **LIGHT-VTP treatment improves vascular function in vivo**

We have previously shown that the fusion compound LIGHT-VTP when injected i.v. into tumor-bearing mice has dual effects on tumor vasculature and the immune environment.<sup>26</sup> To assess its intratumoral effects in GIST, humanized NSG mice were implanted s.c. and treated twice/week with LIGHT-VTP (a 1:1 mixture of human and mouse LIGHT-VTP) starting from a tumor size of approximately 150 mm<sup>3</sup> and continuing until approximately 500 mm<sup>3</sup> (up to 4 weeks treatment). Similarly, humanized NSG mice bearing i.p. implanted GIST were treated twice/week for up to 4 weeks (Figure 4a). At endpoint, vessel functionality was tested by infusing FITC-lectin i.v. and quantifying its binding to CD31<sup>+</sup> vessels as a surrogate marker for tumor perfusion.<sup>12,15</sup> In all LIGHT-VTP-treated tumors, perfusion was significantly increased compared to control groups (Figure 4b). Increased perfusion leads to improved tumor oxygenation which was measured by quantifying intratumoral hypoxia-probe deposits. Figure 4c demonstrates a significant reduction in hypoxic tumor area following LIGHT-VTP treatment in s.c. and i.p. GISTs. The vascular normalization index (as measured by perfusion/hypoxia) and the increase in intratumoral macrophages in GIST grown in non-humanized, immune-deficient NSG mice were comparable to humanized NSG mice (Supplementary Figure S3a–d),<sup>15</sup> thus indicating that LIGHT-induced vascular changes were independent of human adaptive immune cells.

### **LIGHT-VTP treatment increases effector T cell infiltration in humanized GIST mice**

To assess the impact of LIGHT-VTP on the intratumoral, adaptive immune landscape, we focused on the i.p. GIST model since it presented with a higher baseline human CD3<sup>+</sup> T cell infiltration compared to s.c. GIST (Supplementary Figure S4a). In addition, in other cancers such as melanoma, mouse i.p. tumors seem to harbor more TLS compared to s.c. tumors of the same cancer type.<sup>27</sup> Mice were treated with biweekly injections of LIGHT-VTP followed by intratumoral flow cytometry analysis. Figure 5 shows a significant increase in human CD3<sup>+</sup> T cells in LIGHT-VTP treated tumors compared to controls; this correlated with increased numbers of human CD8<sup>+</sup> but not CD4<sup>+</sup> T cells. Importantly, LIGHT-VTP induced intratumoral effector CD8<sup>+</sup> T cells as measured by Ki67 and Granzyme B (GrzB) expression. No statistically significant increase in CD4<sup>+</sup> regulatory or effector T cells was observed (Supplementary Figure S4b and S4c). Although intratumoral B cell numbers did not increase significantly with treatment, there was an upward trend ( $p = 0.12$ ). CD8<sup>+</sup> or CD4<sup>+</sup> T cell populations in peripheral blood remained unchanged before and after treatment (Supplementary Figure S5a and S5b); B cell numbers declined significantly ( $p = 0.0025$ ) in untreated groups throughout the study but still remained abundant within the huCD45<sup>+</sup> cell population (Supplementary Figure S5c). The peritoneal tumor burden was assessed with a mouse scoring system similar to the peritoneal cancer index (PCI) used in humans.<sup>23</sup> The overall tumor burden as measured by PCI score was similar in control versus LIGHT-VTP treated humanized NSG mice (Supplementary Figure S5d). This demonstrates that LIGHT-VTP treatment alone (average injections of 6–8 doses) mobilized effector CD8<sup>+</sup> T cells but did not reduce i.p. tumor burden. This finding is consistent with an adjuvant effect of LIGHT-VTP in immunotherapy in models of pancreatic and lung cancers.<sup>14</sup>

### **LIGHT-VTP treatment induces TLS in humanized GIST mice which resemble spontaneous TLS in patient GIST**

Thus far, we demonstrated that LIGHT-VTP in GIST induced vascular normalization concomitant with an increase in macrophages and cytotoxic effector T cells. Immunohistochemical analysis also showed a significant increase in diffuse CD3<sup>+</sup> T cell infiltration in i.p. GIST tumors following LIGHT-VTP treatment (Figure 6a). Similar to flow cytometry analysis, a trend for an increase in human B cells was observed (Figure 6b). Importantly, while overall diffuse B cell numbers did not reach significance between groups, only LIGHT-VTP treated tumors showed local immune cell clusters consisting of human CD3<sup>+</sup> T cells, human CD20<sup>+</sup> B cells, and HEVs (MECA79<sup>+</sup>) (Figure 6c). This demonstrates that human B cells were recruited to LIGHT-VTP treated GIST, albeit highly localized and in small numbers. These clusters resembled lymphocyte aggregates detectable in some GIST patients (Figure 6d), which show loosely associated T and B cells, the presence of HEVs but absence of a germinal center, indicative of an immature TLS phenotype. These findings demonstrate that targeting LIGHT to the tumor vasculature in GIST increases immune cell infiltration and can trigger the formation of lymphoid aggregates.

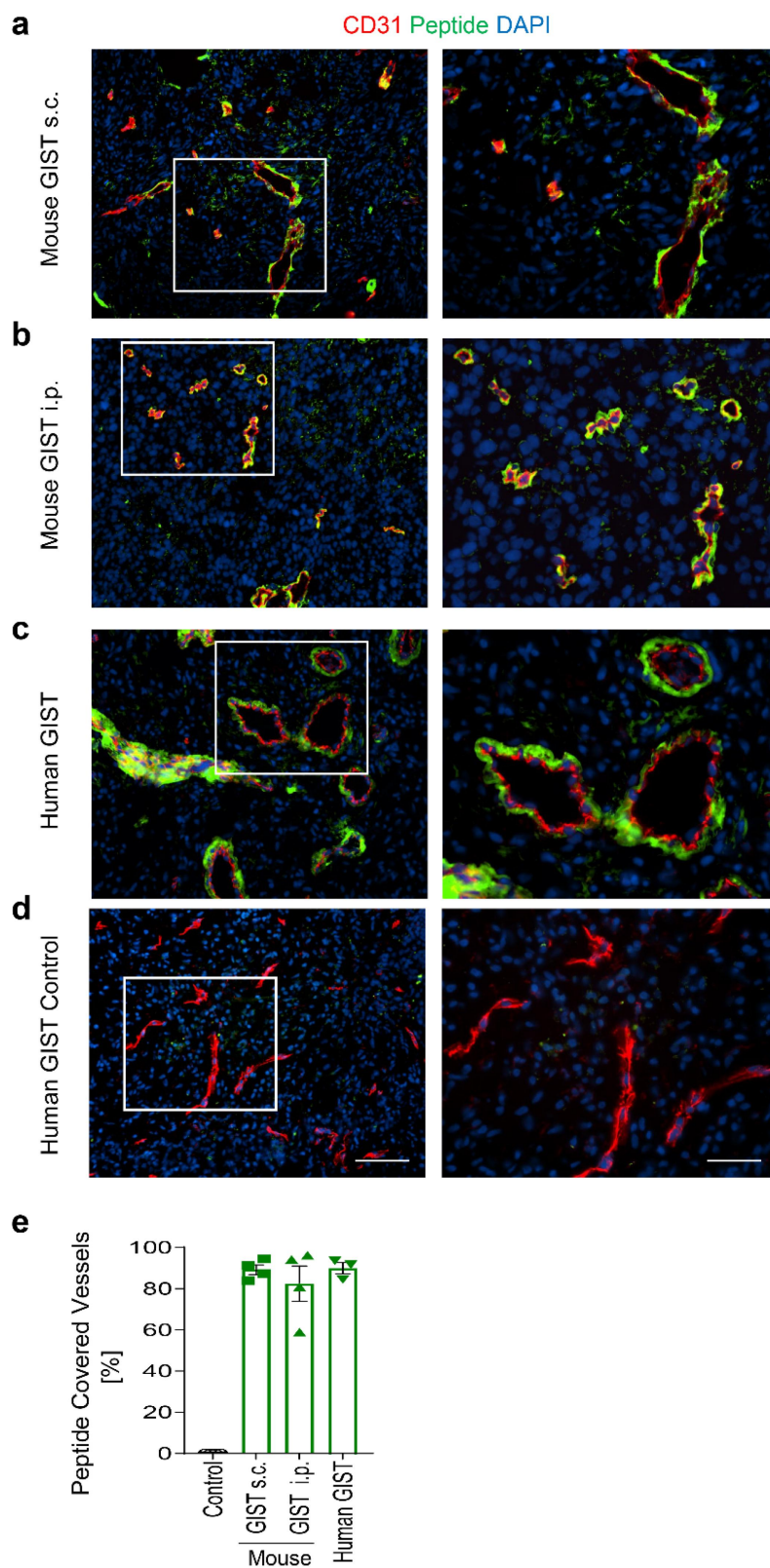


**Figure 3.** Blood vessels in humanized mice and patient GIST are effectively targeted by a tumor-homing peptide. (a – d) Representative images of CGKRK-FAM peptide (green) binding to CD31 (red) blood vessels in (a) s.c. GIST in humanized mice, (b) i.p. GIST in humanized mice, or (c) patient GIST. (d) Patient GIST staining control. Scale bar left, 100  $\mu$ m, scale bar right, 50  $\mu$ m. (e) Quantification of % peptide-covered blood vessels in all tumors,  $n = 3-4$  mice/patients.



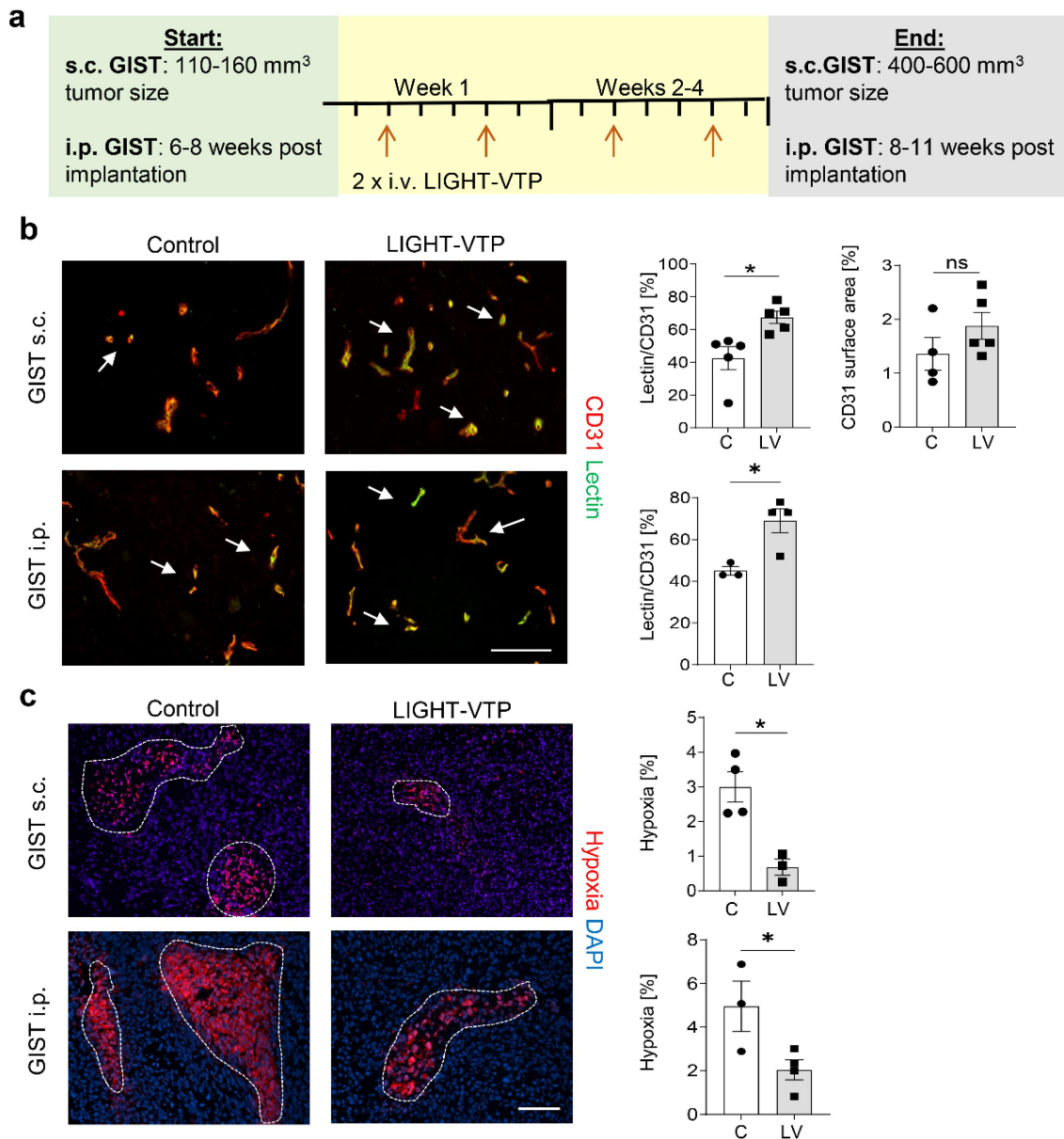


**Figure 4.** LIGHT-VTP treatment induces vascular normalization in s.c. and i.p. GISTs grown in humanized mice. (a) LIGHT-VTP treatment start/end in s.c. and i.p. GIST implanted in humanized NSG mice. (b) Upper (s.c. GIST): representative images depict vascular CD31 expression (red) and infused FITC-lectin (green) as a surrogate marker for tumor perfusion; arrows indicate overlay (yellow) in control (C) or LIGHT-VTP (LV) treated mice. Quantification of overlay and CD31<sup>+</sup> blood vessels,  $n = 4-5$  mice, mean  $\pm$  SEM,  $*p = 0.014$ , Student's  $t$ -test. Lower: i.p. GIST,  $n = 3-4$  mice, mean  $\pm$  SEM,  $*p = 0.019$ , Student's  $t$ -test. Scale bar, 100  $\mu$ m. (c). Imaging and quantification of hypoxia probe (red, white dotted circles). Upper, s.c. GIST:  $n = 3-4$  mice, mean  $\pm$  SEM,  $*p = 0.0085$ , Student's  $t$ -test. Lower, i.p. GIST:  $n = 3-4$  mice, mean  $\pm$  SEM,  $*p = 0.047$ , Student's  $t$ -test. Scale bar, 100  $\mu$ m.

## Discussion

This study demonstrated in humanized mice that the GIST microenvironment can be targeted and modulated to increase immune infiltration and generate cytotoxic effector cells; importantly, this also includes the therapeutic induction of TLS using low dose, nontoxic cytokine therapy.

Current GIST mouse models employ primary cells derived from GIST patients or patient-derived tumor tissue, which are implanted into immunodeficient mice. Alternatively, transgenic immunocompetent mice with specific gene mutations are available but most commonly develop lesions in the cecum and therefore do not fully recapitulate features of human GIST.<sup>3</sup> Here, we generated a CD34<sup>+</sup> cord blood

humanized mouse model, which was implanted with human GIST-T1 cells to specifically study the capacity of LIGHT-VTP to modulate the GIST immune environment. At different sites of tumor implantation, mimicking locally restricted versus peritoneal disseminated cancer growth, the GIST morphological features were largely preserved when compared to a c-KIT mutant human gastric GIST of mixed phenotype. There was a marked difference in spontaneous human CD3<sup>+</sup> T cell infiltration, which was stronger in i.p. tumors. This finding is consistent with the observation that metastatic GIST to liver and peritoneum harbor more CD3<sup>+</sup> T cells.<sup>5</sup> T cells and CD56<sup>bright</sup> NK cells are major components of the human GIST immune environment and independently predict progression free survival in imatinib-treated local GIST



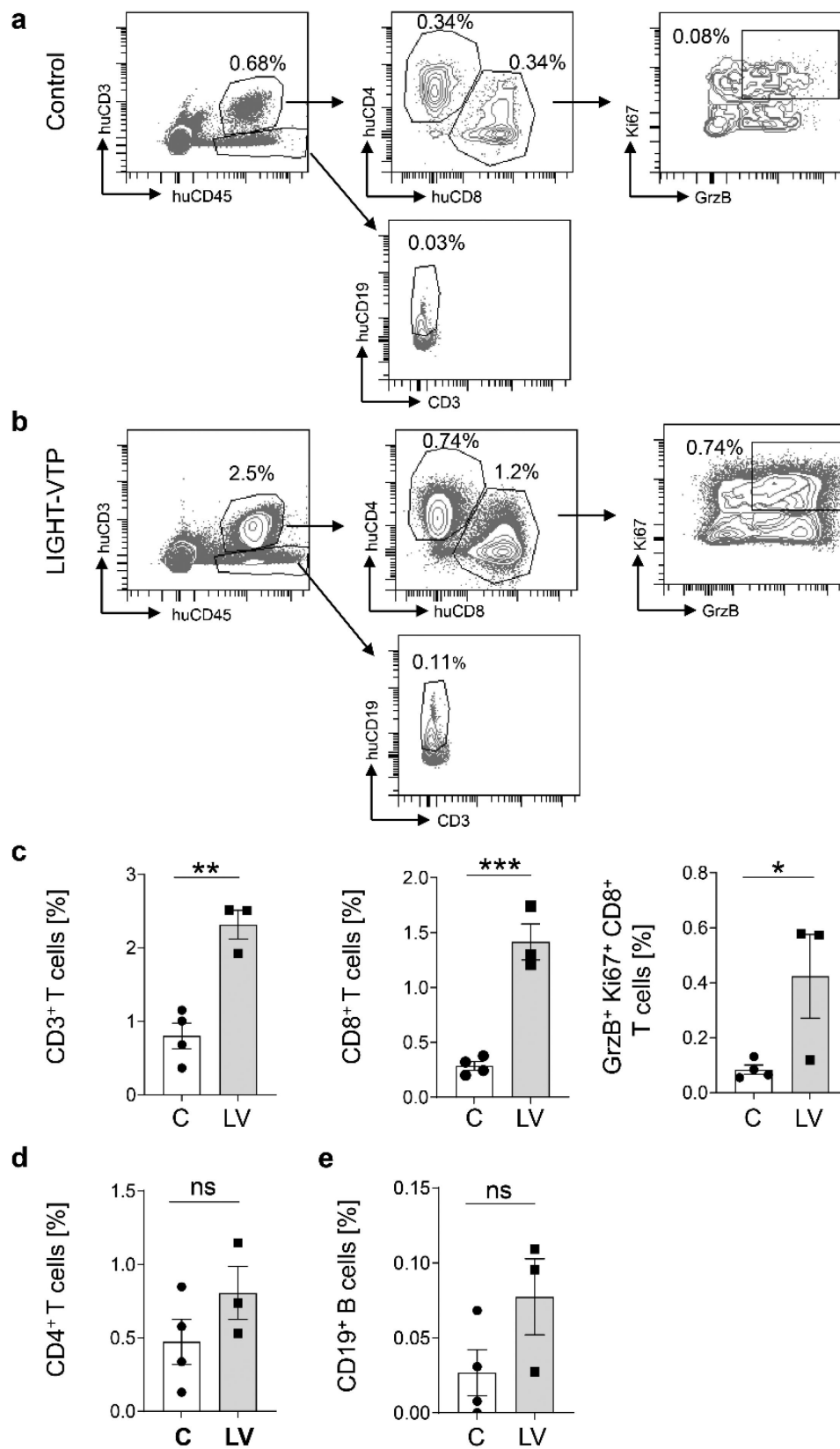


**Figure 5.** LIGHT-VTP treatment induces intratumoral effector CD8<sup>+</sup> T cells. (a and b) Representative flow cytometry graphs displaying the gating strategy for human CD45<sup>+</sup>, CD3<sup>+</sup>, CD4<sup>+</sup>, CD8<sup>+</sup>, CD8<sup>+</sup>Ki67<sup>+</sup>GrzB<sup>+</sup> intratumoral T cells and CD19<sup>+</sup> B cells in i.p. GIST in (a) control and (b) LIGHT-VTP treated mice. (c) Quantification of human CD3<sup>+</sup> T cells (\*\* $p = 0.0023$ ), CD8<sup>+</sup> T cells (\*\*\* $p = 0.0006$ ), and CD8<sup>+</sup>Ki67<sup>+</sup>GrzB<sup>+</sup> effector T cells (\* $p = 0.046$ ), gated on live cells, in control (C) or LIGHT-VTP (LV) treated i.p. GIST. (d) Quantification of CD4<sup>+</sup> T cells (ns,  $p = 0.22$ ) and (e) CD19<sup>+</sup> B cells (ns,  $p = 0.12$ ) gated on live cells in C and LV treated groups. For all groups,  $n = 3-4$  mice, mean  $\pm$  SEM, Student's  $t$ -test.

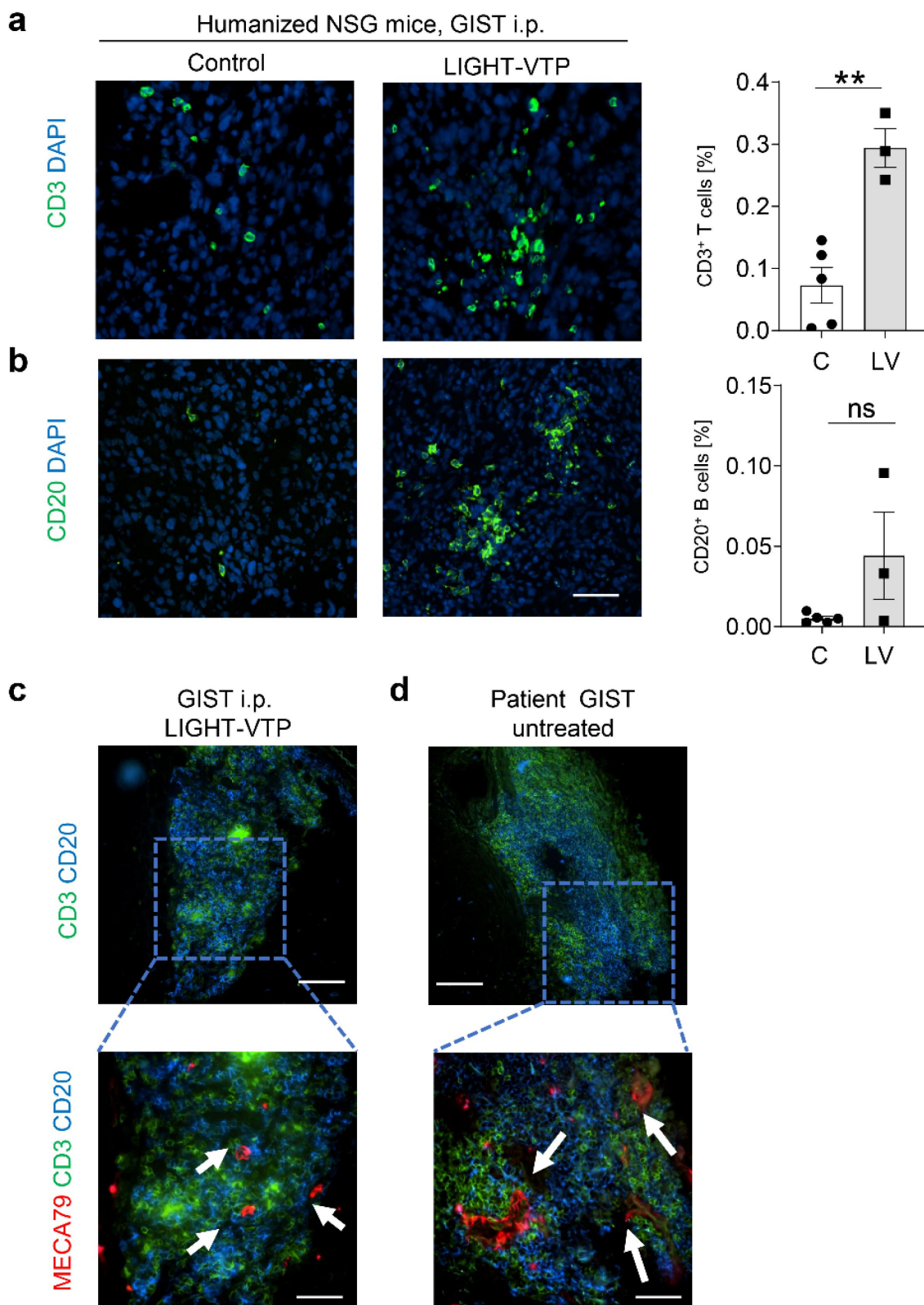


**Figure 6.** LIGHT-VTP treatment induces T cell infiltration and TLS formation in i.p. GIST tumors. (a) Representative images of human CD3<sup>+</sup> T cells in control (C) and LIGHT-VTP (LV) treated humanized mice bearing i.p. GIST, and quantification of intratumoral infiltration,  $n = 3-5$ ,  $**p = 0.0025$ , mean  $\pm$  SEM, Student's  $t$ -test. Scale bar, 50  $\mu$ m. (b) Representative images of human CD20<sup>+</sup> B cells in control (C) and LIGHT-VTP (LV) treated mice, and quantification of intratumoral infiltration,  $n = 3-5$ ,  $ns, p = 0.1$ , mean  $\pm$  SEM, Student's  $t$ -test. Scale bar, 50  $\mu$ m. (c) Representative images of a T cell (green) and B cell (blue) cluster in LIGHT-VTP treated i.p. GIST (upper), scale bar 100  $\mu$ m; (lower) magnified area also including MECA79<sup>+</sup> HEVs (red, indicated by arrows), scale bar, 50  $\mu$ m. (d) Representative images of a spontaneous T cell (green) and B cell (blue) cluster in a patient GIST (upper), scale bar 100  $\mu$ m; (lower) magnified area also including MECA79<sup>+</sup> HEVs (red, indicated by arrows), scale bar 50  $\mu$ m.

specimens.<sup>6</sup> In contrast, the accumulation of CD68<sup>+</sup> macrophages correlates with high risk and metastatic GIST.<sup>3,28</sup> While CD68<sup>+</sup> macrophages were present in human and humanized mouse GISTs, CD56<sup>+</sup> NK cells were largely absent in GIST grown in humanized mice. This suggests an engraftment insufficiency during humanization which is also reflected in low numbers of CD14<sup>+</sup> monocytes in blood, spleen, and bone marrow at 16 weeks post-engraftment when compared to lymphoid lineages such as T and B cells. NSG mice have been shown to successfully develop B cell-dominated grafts; however, the development of myeloid lineages is compromised in the absence of human cytokines such as stem cell factor (SCF), granulocyte-macrophage colony-stimulating factor (GM-CSF), or interleukin (IL)3.<sup>24</sup> The next generation of transgenic mice expressing a combination of these factors, e.g., NSG-SGM3 or MISTRG mice, shows higher levels of multi-lineage human hematopoietic engraftment with superior representation of innate immune cell lineages.<sup>29,30</sup> However, graft-versus-host disease-related erythropenia leads to severe anemia in these mice, which makes long-term tumor progression studies challenging.<sup>29</sup> The field is rapidly evolving with the development of highly sophisticated, but cost-intensive humanized mouse models, which include for instance co-implantation of CD34<sup>+</sup> stem cells with thymus and transient human cytokine expression.<sup>31</sup>

While the decreased innate immune compartment likely affects the functionality of the graft as a whole, the focus of this LIGHT-VTP study was on the lymphoid cells. To this end, NSG and humanized NSG mice were treated with a dose of LIGHT-VTP which has previously been shown to remodel vasculature in syngeneic mouse cancer models.<sup>12,13,15</sup> Since VTP binding to human GIST implanted in mice is highly efficient, LIGHT-VTP treatment indeed increased overall tumor perfusion and reduced hypoxia which are both readouts for vessel normalization and improved vascular function.

Normalization of the angiogenic vasculature and accompanying microenvironmental changes have been shown to support Th1-driven anti-tumor immunity.<sup>32–34</sup> Using our humanized GIST system, we demonstrated that i.p. tumors were significantly infiltrated by human CD3<sup>+</sup> T cells and harbored highly proliferative effector CD8<sup>+</sup> T cells. Moreover, lymphoid aggregates resembling TLS were identified in mouse i.p. GIST following LIGHT-VTP treatment and are similar in composition to TLS that can form spontaneously in human gastric GIST. Remarkably, HEVs arise in tumors in humanized mice where vessels are of mouse origin but infiltrating immune cells are of human origin. Given the absence of NK cells in these tumors, it is conceivable that vessel normalization supports HEV formation from postcapillary venules which is maintained by human T cells.<sup>16</sup>

Some tumors, in particular those with a substantial mutational load, can recruit and activate naive anti-tumor lymphocytes via TLS.<sup>35–37</sup> In a Chinese cohort of 118 GIST patients, approximately 45% showed histopathological features of TLS, with the majority displaying small lymphocyte clusters. Although CD20<sup>+</sup> B cell numbers are low in GIST,<sup>5</sup> a small number of patients (6%) present with mature TLS which also include germinal centers.<sup>10</sup> In that study, the location of TLS within the GIST and the presence of HEVs were not analyzed.<sup>10</sup>

Crucially, however, the presence of spontaneous TLS in GIST patients was an independent prognostic factor for overall survival and time to recurrence, while the maturity of TLS seemed to negatively correlate with imatinib resistance. In other cancers, including melanoma, soft-tissue sarcoma, and renal cell carcinoma, the presence of spontaneously arising TLS has been shown to predict the response to checkpoint inhibitors.<sup>38–40</sup> So far, however, there are few tools available to therapeutically induce TLS. Thus, our finding that LIGHT-VTP can induce TLS and effector T cells is of high relevance for future immunotherapy in GIST and a promising example for the successful application of cytokine therapeutics.<sup>41</sup> In combination with checkpoint inhibitors or vaccination, these TLS are likely to mature further and set the stage for stronger anti-cancer immunity.<sup>14</sup>

## Acknowledgments

We thank Mitchell Owens for technical assistance, the Radiation Oncology staff at Sir Charles Gairdner Hospital for help with mouse irradiation and acknowledge the support of the Harry Perkins Institute FACS facility. This work was supported by the Cancer Council of Western Australia under Grants 682 and 1034, the National Health and Medical Research Council (NHMRC) APP2001120, and Cancer Program funds from the Harry Perkins Institute of Medical Research.

## Disclosure statement

No potential conflict of interest was reported by the author(s).

## Funding

This work was supported by the Cancer Council of Western Australia under Grants 682 and 1034, the National Health and Medical Research Council (NHMRC) APP2001120, and Cancer Program funds from the Harry Perkins Institute of Medical Research.

## ORCID

Ruth Ganss  <http://orcid.org/0000-0002-5551-045X>

## Data availability statement

The data that support the findings of this study are available from the corresponding author upon reasonable request.

## References

- Demetri GD, von Mehren M, Blanke CD, Van den Abbeele AD, Eisenberg B, Roberts PJ, Heinrich MC, Tuveson DA, Singer S, Janicek M, et al. Efficacy and safety of imatinib mesylate in advanced gastrointestinal stromal tumors. *N Engl J Med.* 2002;347:472–480. doi:10.1056/NEJMoa020461.
- Fiorino E, Merlini A, D'Ambrosio L, Cerviere I, Berrino E, Marchio C, Giraudo L, Basirico M, Massa A, Donini C, et al. Integrated antitumor activities of cellular immunotherapy with CIK lymphocytes and Interferons against KIT/PDGFRα wild type GIST. *Int J Mol Sci.* 2022;23. doi:10.3390/ijms231810368.
- Li B, Chen H, Yang S, Chen F, Xu L, Li Y, Li M, Zhu C, Shao F, Zhang X, et al. Advances in immunology and immunotherapy for mesenchymal gastrointestinal cancers. *Mol Cancer.* 2023;22:71. doi:10.1186/s12943-023-01770-6.



4. Arshad J, Costa PA, Barreto-Coelho P, Valdes BN, Trent JC. Immunotherapy strategies for gastrointestinal stromal tumor. *Cancers (Basel)*. 2021;13. doi:10.3390/cancers13143525.
5. Cameron S, Gieselmann M, Blaschke M, Ramadori G, Fuzesi L. Immune cells in primary and metastatic gastrointestinal stromal tumors (GIST). *Int J Clin Exp Pathol*. 2014;7:3563–3579.
6. Rusakiewicz S, Semeraro M, Sarabi M, Desbois M, Locher C, Mendez R, Vimond N, Concha A, Garrido F, Isambert N, et al. Immune infiltrates are prognostic factors in localized gastrointestinal stromal tumors. *Cancer Res*. 2013;73:3499–3510. doi:10.1158/0008-5472.CAN-13-0371.
7. Pantaleo MA, Tarantino G, Agostinelli C, Urbini M, Nannini M, Saponara M, Castelli C, Stacchiotti S, Fumagalli E, Gatto L, et al. Immune microenvironment profiling of gastrointestinal stromal tumors (GIST) shows gene expression patterns associated to immune checkpoint inhibitors response. *Oncoimmunology*. 2019;8:e1617588. doi:10.1080/2162402X.2019.1617588.
8. Balachandran VP, Cavnar MJ, Zeng S, Bamboat ZM, Ocuin LM, Obaid H, Sorenson EC, Popow R, Ariyan C, Rossi F, et al. Imatinib potentiates antitumor T cell responses in gastrointestinal stromal tumor through the inhibition of Ido. *Nat Med*. 2011;17(9):1094–1100. doi:10.1038/nm.2438.
9. Seifert AM, Zeng S, Zhang JQ, Kim TS, Cohen NA, Beckman MJ, Medina BD, Maltbaek JH, Loo JK, Crawley MH, et al. Blockade enhances T-cell activity and antitumor efficacy of imatinib in gastrointestinal stromal tumors. *Clin Cancer Res*. 2017;23, 454–465. 1078-0432. D-1/PD-L1. doi:10.1158/1078-0432.CCR-16-1163.
10. Lin Q, Tao P, Wang J, Ma L, Jiang Q, Li J, Zhang G, Liu J, Zhang Y, Hou Y, et al. Tumor-associated tertiary lymphoid structure predicts postoperative outcomes in patients with primary gastrointestinal stromal tumors. *Oncoimmunology*. 2020;9:1747339. doi:10.1080/2162402X.2020.
11. Johansson-Percival A, Ganss R. Therapeutic induction of tertiary lymphoid structures in cancer through stromal remodeling. *Front Immunol*. 2021;12:674375. doi:10.3389/fimmu.2021.674375.
12. He B, Jabouille A, Steri V, Johansson-Percival A, Michael IP, Kotamraju VR, Junckerstorff R, Nowak AK, Hamzah J, Lee G, et al. Vascular targeting of LIGHT normalizes blood vessels in primary brain cancer and induces intratumoural high endothelial venules. *J Pathol*. 2018;245(2):209–221. doi:10.1002/path.5080.
13. He B, Johansson-Percival A, Backhouse J, Li J, Lee GYF, Hamzah J, Ganss R. Remodeling of metastatic vasculature reduces lung colonization and sensitizes overt metastases to immunotherapy. *Cell Rep*. 2020;30(3):714–724. doi:10.1016/j.celrep.2019.12.013.
14. Johansson-Percival A, He B, Li ZJ, Kjellen A, Russell K, Li J, Larma I, Ganss R. De Novo induction of intratumoral lymphoid structures and vessel normalization enhances immunotherapy in resistant tumors. *Nat Immunol*. 2017;18(11):1207–1217. doi:10.1038/ni.3836.
15. Johansson-Percival A, Li ZJ, Lakhiani DD, He B, Wang X, Hamzah J, Ganss R. Intratumoral LIGHT restores pericyte contractile properties and vessel integrity. *Cell Rep*. 2015;13:2687–2698. doi:10.1016/j.celrep.2015.12.004.
16. Hua Y, Vella G, Rambow F, Allen E, Antoranz Martinez A, Duhamel M, Takeda A, Jalkanen S, Junius S, Smeets A, et al. Cancer immunotherapies transition endothelial cells into HEVs that generate TCF1+ T lymphocyte niches through a feed-forward loop. *Cancer Cell*. 2022;40(12):1600–1618. doi:10.1016/j.ccell.2022.11.002.
17. Rosato RR, Davila-Gonzalez D, Choi DS, Qian W, Chen W, Kozielski AJ, Wong H, Dave B, Chang JC. Evaluation of anti-PD-1-based therapy against triple-negative breast cancer patient-derived xenograft tumors engrafted in humanized mouse models. *Breast Cancer Res*. 2018;20:108. doi:10.1186/s13058-018-1037-4.
18. Capasso A, Lang J, Pitts TM, Jordan KR, Lieu CH, Davis SL, Diamond JR, Kopetz S, Barbee J, Peterson J, et al. Characterization of immune responses to anti-PD-1 mono and combination immunotherapy in hematopoietic humanized mice implanted with tumor xenografts. *J Immunother Cancer*. 2019;7:37. doi:10.1186/s40425-019-0518-z.
19. Taguchi T, Sonobe H, Toyonaga S, Yamasaki I, Shuin T, Takano A, Araki K, Akimaru K, Yuri K. Conventional and molecular cytogenetic characterization of a new human cell line, GIST-T1, established from gastrointestinal stromal tumor. *Lab Invest*. 2002;82(5):663–665. doi:10.1038/labinvest.3780461.
20. Kekarainen T, Mannelin S, Laine J, Jaatinen T. Optimization of immunomagnetic separation for cord blood-derived hematopoietic stem cells. *BMC Cell Biol*. 2006;7:30. doi:10.1186/1471-2121-7-30.
21. Agemy L, Friedmann-Morvinski D, Kotamraju VR, Roth L, Sugahara KN, Girard OM, Mattrey RF, Verma IM, Ruoslahti E. Targeted nanoparticle enhanced proapoptotic peptide as potential therapy for glioblastoma. *Proc Natl Acad Sci U S A*. 2011;108:17450–17455. doi:10.1073/pnas.1114518108.
22. Miettinen M, Lasota J. Gastrointestinal stromal tumors: review on morphology, molecular pathology, prognosis, and differential diagnosis. *Arch Pathol Lab Med*. 2006;130:1466–1478. doi:10.5858/2006-130-1466-GSTROM.
23. Bastiaenen VP, Klaver CEL, van der Heijden MCS, Nijman LE, Lecca MC, Tanis PJ, Lenos KJ, Vermeulen L. A mouse model for peritoneal metastases of colorectal origin recapitulates patient heterogeneity. *Lab Invest*. 2020;100(11):1465–1474. doi:10.1038/s41374-020-0448-x.
24. Wunderlich M, Chou FS, Sexton C, Presicce P, Choungnet CA, Aliberti J, Mulloy JC. Improved multilineage human hematopoietic reconstitution and function in NSGS mice. *PLOS ONE*. 2018;13: e0209034. doi:10.1371/journal.pone.0209034.
25. Johansson A, Hamzah J, Ganss R. License for destruction: tumor-specific cytokine targeting. *Trends Mol Med*. 2014;20(1):16–24. doi:10.1016/j.molmed.2013.10.002.
26. Johansson-Percival A, He B, Ganss R. Immunomodulation of tumor vessels: it takes two to tango. *Trends Immunol*. 2018;39:801–814. doi:10.1016/j.it.2018.08.001.
27. Rodriguez AB, Peske JD, Woods AN, Leick KM, Mauldin IS, Meneveau MO, Young SJ, Lindsay RS, Melsen MM, Cyranowski S, et al. Immune mechanisms orchestrate tertiary lymphoid structures in tumors via cancer-associated fibroblasts. *Cell Rep*. 2021;36:109422. doi:10.1016/j.celrep.2021.109422.
28. van Dongen M, Savage ND, Jordanova ES, Briaire-de Bruijn IH, Walburg KV, Ottenhoff TH, Hogendoorn PC, van der Burg SH, Gelderblom H, van Hall T. Anti-inflammatory M2 type macrophages characterize metastasized and tyrosine kinase inhibitor-treated gastrointestinal stromal tumors. *Int J Cancer*. 2010;127(4):899–909. doi:10.1002/ijc.25113.
29. Rongvaux A, Willinger T, Martinek J, Strowig T, Gearty SV, Teichmann LL, Saito Y, Marches F, Halene S, Palucka AK, et al. Development and function of human innate immune cells in a humanized mouse model. *Nat Biotechnol*. 2014;32(4):364–372. doi:10.1038/nbt.2858.
30. Sippel TR, Radtke S, Olsen TM, Kiem HP, Rongvaux A. Human hematopoietic stem cell maintenance and myeloid cell development in next-generation humanized mouse models. *Blood Adv*. 2019;3:268–274. doi:10.1182/bloodadvances.2018023887.
31. Somasundaram R, Connelly T, Choi R, Choi H, Samarkina A, Li L, Gregorio E, Chen Y, Thakur R, Abdel-Mohsen M, et al. Tumor-infiltrating mast cells are associated with resistance to anti-PD-1 therapy. *Nat Commun*. 2021;12:346. doi:10.1038/s41467-020-20600-7.
32. Hamzah J, Jugold M, Kiessling F, Rigby P, Manzur M, Marti HH, Rabie T, Kaden S, Grone HJ, Hammerling GJ, et al. Vascular normalization in Rgs5-deficient tumours promotes immune destruction. *Nature*. 2008;453(7193):410–414. doi:10.1038/nature06868.
33. Tian L, Goldstein A, Wang H, Ching Lo H, Sun Kim I, Welte T, Sheng K, Dobrolecki LE, Zhang X, Putluri N, et al. Mutual regulation of tumour vessel normalization and immunostimulatory reprogramming. *Nature*. 2017;544(7649):250–254. doi:10.1038/nature21724.

34. Zheng X, Fang Z, Liu X, Deng S, Zhou P, Wang X, Zhang C, Yin R, Hu H, Chen X, et al. Increased vessel perfusion predicts the efficacy of immune checkpoint blockade. *J Clin Invest.* 2018;128:2104–2115. doi:10.1172/JCI96582.
35. Thompson ED, Enriquez HL, Fu YX, Engelhard VH. Tumor masses support naive T cell infiltration, activation, and differentiation into effectors. *J Exp Med.* 2010;207:1791–1804. doi:10.1084/jem.20092454.
36. Peske JD, Thompson ED, Gemta L, Baylis RA, Fu YX, Engelhard VH. Effector lymphocyte-induced lymph node-like vasculature enables naive T-cell entry into tumours and enhanced anti-tumour immunity. *Nat Commun.* 2015;6:7114. doi:10.1038/ncomms8114.
37. Schumacher TN, Thommen DS. Tertiary lymphoid structures in cancer. *Science.* 2022;375:eabf9419. doi:10.1126/science.abf9419.
38. Helmink BA, Reddy SM, Gao J, Zhang S, Basar R, Thakur R, Yizhak K, Sade-Feldman M, Blando J, Han G, et al. B cells and tertiary lymphoid structures promote immunotherapy response. *Nature.* 2020;577(7791):549–555. doi:10.1038/s41586-019-1922-8.
39. Petitprez F, de Reynies A, Keung EZ, Chen TW, Sun CM, Calderaro J, Jeng YM, Hsiao LP, Lacroix L, Bougouin A, et al. B cells are associated with survival and immunotherapy response in sarcoma. *Nature.* 2020;577(7791):556–560. doi:10.1038/s41586-019-1906-8.
40. Cabrita R, Lauss M, Sanna A, Donia M, Skaarup Larsen M, Mitra S, Johansson I, Phung B, Harbst K, Vallon-Christersson J, et al. Tertiary lymphoid structures improve immunotherapy and survival in melanoma. *Nature.* 2020;577:561–565. doi:10.1038/s41586-019-1914-8.
41. Deckers J, Anbergen T, Hokke AM, de Dreu A, Schrijver DP, de Bruin K, Toner YC, Beldman TJ, Spangler JB, de Greef TFA, et al. Engineering cytokine therapeutics. *Nat Rev Bioeng.* 2023;1(4):286–303. doi:10.1038/s44222-023-00030-y.